agriculture

MDPI

Article

Analyzing Safety Factors and Predicting Fatigue Life of Weak Points in an Electrically Driven, Multi-Purpose Cultivation Tractor

In-Seok Hwang [1], Jeong-Hun Kim [2,3], Wan-Tae Im [1], Hwan-Hong Jeung [4], Ju-Seok Nam [2,3,*] and Chang-Seop Shin [1,*]

[1] Department of Biosystems Engineering, Chungbuk National University, Cheongju 28644, Republic of Korea; his3007@chungbuk.ac.kr (I.-S.H.); wnatae8878@gmail.com (W.-T.I.)
[2] Department of Biosystems Engineering, Kangwon National University, Chuncheon 24341, Republic of Korea; jhkim1995@kangwon.ac.kr
[3] Interdisciplinary Program in Smart Agriculture, Kangwon National University, Chuncheon 24341, Republic of Korea
[4] Cheung Won SFA Co., Ltd., Seoul 08389, Republic of Korea; jeung.hh@cwsfa.co.kr
* Correspondence: njsg1218@kangwon.ac.kr (J.-S.N.); shinchang7@chungbuk.ac.kr (C.-S.S.); Tel.: +82-33-250-6497 (J.-S.N.); +82-43-261-2584 (C.-S.S.)

Abstract: The advancement of agriculture and a shortage of labor have led to an increased use of agricultural machinery. However, the resulting environmental issues have prompted a shift from internal combustion engines to electric drivetrains. The electric drivetrain includes the installation of batteries, which can lead to decreased energy efficiency and significant loads on the vehicle due to their heavy weight. Consequently, the importance of ensuring the safety of agricultural machinery is being increasingly emphasized. The load on the frame of agricultural machinery is not consistent during off-road driving, and the accumulation of load cycles can lead to the destruction and failure of components. Therefore, it is necessary to ensure a level of safety and to predict the fatigue life. In this study, we estimate the safety factor and predict the fatigue life of weak points in an electrically driven, multi-purpose cultivation tractor based on working conditions (width, soil, and drive). Strain gauges were attached to these weak points to measure the strain, which was then converted to von Mises stress. Fatigue life was predicted using the rainflow counting method and the Palmgren–Miner rule. The results showed that the safety factor measured under various working conditions was greater than 1. The estimated minimum fatigue life was 124,176 years. Considering that the cultivator is used for 29.7 h annually and has a durability lifespan of 5 years, it is expected to be safely usable throughout its service life.

Keywords: electrically driven; multi-purpose cultivation tractor; fatigue life; rainflow counting; safety factor

check for updates

Citation: Hwang, I.-S.; Kim, J.-H.; Im, W.-T.; Jeung, H.-H.; Nam, J.-S.; Shin, C.-S. Analyzing Safety Factors and Predicting Fatigue Life of Weak Points in an Electrically Driven, Multi-Purpose Cultivation Tractor. *Agriculture* **2024**, *14*, 416. https://doi.org/10.3390/agriculture14030416

Academic Editor: Jin Yuan

Received: 13 January 2024
Revised: 28 February 2024
Accepted: 28 February 2024
Published: 5 March 2024

Copyright: © 2024 by the authors. Licensee MDPI, Basel, Switzerland. This article is an open access article distributed under the terms and conditions of the Creative Commons Attribution (CC BY) license (https://creativecommons.org/licenses/by/4.0/).

1. Introduction

Recently, a trend of aging agricultural labor forces has been observed in various regions around the world [1–7]. This aging phenomenon has emerged due to a lack of young people entering the agricultural sector and a decline in birth rates. Elderly farmers continue their agricultural activities based on years of experience, yet changes in physical and cognitive abilities may make them more susceptible to accidents during farming operations. This aging trend is intertwined with the sophistication of the agricultural sector and labor shortages, leading to an increase in the use of agricultural machinery. Ronald and Andrew [8] analyzed 115 countries from 2006 to 2010 and found that as the population ages, agricultural labor shortages will lead to technological advances and productivity gains. Consequently, the importance of ensuring the safety of agricultural machinery has been emphasized as the use of agricultural machinery has increased due to agricultural intensification and labor

shortages. Although the risk perception among farmers is relatively low, the incidence of safety accidents in the agricultural sector is trending high due to the dangerous working environment compared to other industries [9,10]. Elderly farmers necessitate heightened attention towards work efficiency and safety management, which can significantly affect agricultural productivity and sustainability. Accidents in agricultural settings can often result in serious injury or death, making safety measures essential in the use and care of agricultural machinery. As a result, agricultural machinery manufacturers should focus on designing safer machines and testing the safety of manufactured machines.

Among agricultural machinery, cultivation tractors are used for small- and medium-scale paddy and field farming by attaching various agricultural implements to the main body, and the load on the frame is not consistent when driving off-road. In order to ensure safe farming, it is important to consider the optimal design of the frame. Fatigue damage is an important issue in mechanical design, and components must be designed to withstand cyclic loads [11]. Agricultural machinery experiences frequent failures due to the heavy loads applied. Additionally, the accumulation of large load cycles can lead to destruction and failure of the component [12–14]. The failure that occurs due to the accumulation of fatigue damage is called fatigue failure. Fatigue failures primarily occur due to cracking. The first stage of fatigue failure, the crack, occurs due to local plastic deformation within the material. The crack grows due to repetitive loading and eventually leads to the failure of the material. In this case, the number of load repetitions or the time until the material subjected to cyclic loading failures is known as the fatigue life [15]. Therefore, predicting fatigue life should be considered in the early stages of machine design. This plays a crucial role in accurately assessing the lifespan of components, selecting appropriate materials, ensuring sufficient strength, and establishing efficient maintenance plans. In the field of agriculture, there is a growing emphasis on agricultural machinery design that considers safety and durability, and these efforts are expected to contribute to enhancing the safety and efficiency of agricultural operations. Many studies have been conducted on fatigue life prediction in relation to the safety of machinery. Baek et al. [16] analyzed strain gauge data from the end beam of a freight car bogie to calculate fatigue cycles and used the rainflow counting method to estimate cumulative damage under actual load conditions. This method was found to correspond well with the actual fatigue life, with an error range of 2.7% to 31%. Djebli et al. [17] proposed a fatigue damage accumulation method by applying the energy parameters of the fatigue process. The cycles were calculated using the rainflow counting algorithm and the damage was accumulated according to the Palmgren–Miner rule. The experimental verification results showed that the fatigue life calculation results using the proposed model and the experimental results were in satisfactory agreement. The predicted and experimental lifetimes were found to be in good agreement. Cui et al. [18] developed an integrated fatigue life prediction method for offshore structures. By establishing the crack growth rate relationship and using the proposed method, many influencing factors observed in fatigue testing can be reflected. Kebir et al. [19] used software to simulate fatigue damage under variable loading by considering the effect of average stress on fatigue life and evaluating fatigue damage using the rainflow counting method, and this was confirmed through comparison with results from the literature.

Recently, issues related to global warming have been on the rise, primarily due to an increase in greenhouse gas emissions, including carbon dioxide, and the depletion of fossil fuels. In response to these environmental concerns, research focused on reducing exhaust gas emissions and decreasing dependency on fossil fuels has been actively pursued [20–22]. Such research is particularly important for increasing energy efficiency in agriculture [23–26], which has recently seen a shift from internal combustion engines to electric drive systems [27,28]. With the increasing development and integration of renewable energy sources, electric drive systems are becoming a greener alternative. This can contribute to increasing the sustainability of energy systems and reducing environmental impact in the long term. However, this transition comes with technical, economic, and social challenges, one of which is the reduced energy efficiency and increased load on

vehicles due to heavier batteries compared to internal combustion engines [29,30]. Therefore, additional research and testing are needed to improve the safety and efficiency of these systems. Such efforts are crucial in mitigating the problems of global warming and reducing the consumption of fossil fuels.

The purpose of this study is to analyze the safety of an electrically driven, multi-purpose cultivation tractor by calculating the safety factor. Additionally, it aims to predict the fatigue life based on various working conditions. The safety factor is calculated using the maximum stress measured under each condition. The prediction of fatigue life involves measuring the strain at weak points with attached strain gauges, converting this strain into stress, and then applying the rainflow counting method and the Palmgren–Miner rule [31,32].

2. Materials and Methods

2.1. Electrically Driven, Multi-Purpose Cultivation Tractor

The shape and main specifications of the electrically driven, multi-purpose cultivation tractor used in this study are shown in Figure 1 and Table 1. The ride-on mower used in this study is designed to be adjustable in width for multi-purpose farming, as shown in Figure 2. The load distribution changes with the width, so it was intended to measure the load during operation based on the maximum/minimum width to verify safety.

Figure 1. Shape of the electrically driven, multi-purpose cultivation tractor.

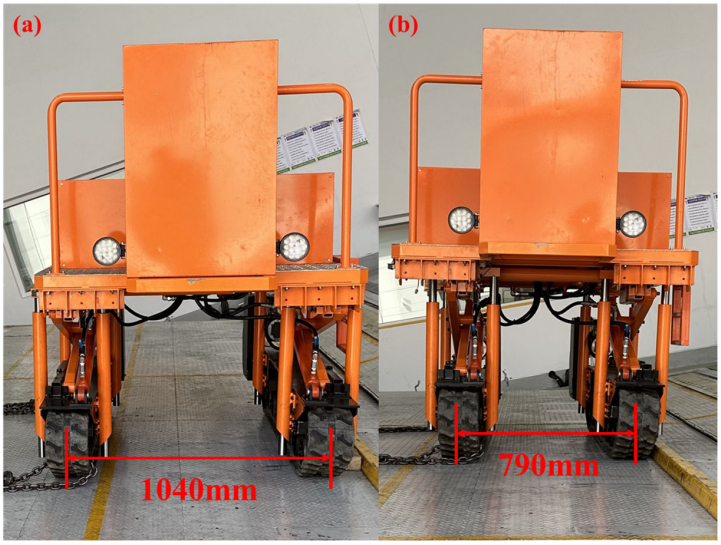

Figure 2. Adjusting the width: (**a**) maximum; (**b**) minimum.

Table 1. Specifications of the tractor.

Items	Specifications
Model	CW-322044-3
Manufacturer/Nation	CWSFA/Korea
Length/Width/Height (mm)	2250/1390/1810
Weight (kg)	1105
Types of Wheels	Caterpillar tracks
Track Size (L/W/H) (mm)	1900/180/365

2.2. Stress Measurement

2.2.1. Mechanical Properties of Materials

In this study, the link connecting the running gear to the plate was selected as the weak link based on the static load analysis and the opinion of metrology experts. The weak link is shown in Figure 3. It is made of stainless steel 400, and the mechanical properties of the material are shown in Table 2.

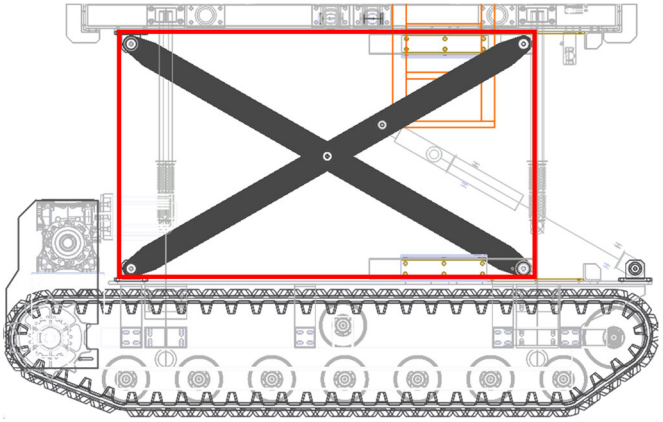

Figure 3. Weakness parts.

Table 2. Mechanical properties of stainless steel 400.

Material	Properties	Value
Stainless Streel 400	Young's modulus (GPa)	196
	Poisson's ratio	0.26
	Density (kg/m^3)	7800
	Ultimate tensile strength (MPa)	420
	Yield strength (MPa)	250

2.2.2. Measurement System

An instrumentation system was built to measure the stresses applied to the vulnerable parts of the controller during driving. Figure 4a shows the measurement system. The measurement system consists of a triaxial strain gauge (KFGS-1-350D17-11 L5M3S, KYOWA, Japan), a data acquisition unit (DAQ, Gantner, Austria), a laptop, and a battery pack. The attachment point of the strain gauge is shown in Figure 4b. The measured values from the strain gauge were transmitted to the laptop via the data acquisition device at a sampling rate of 100 Hz and analyzed using data acquisition software (Dewesoft 2021.6, Slovenia).

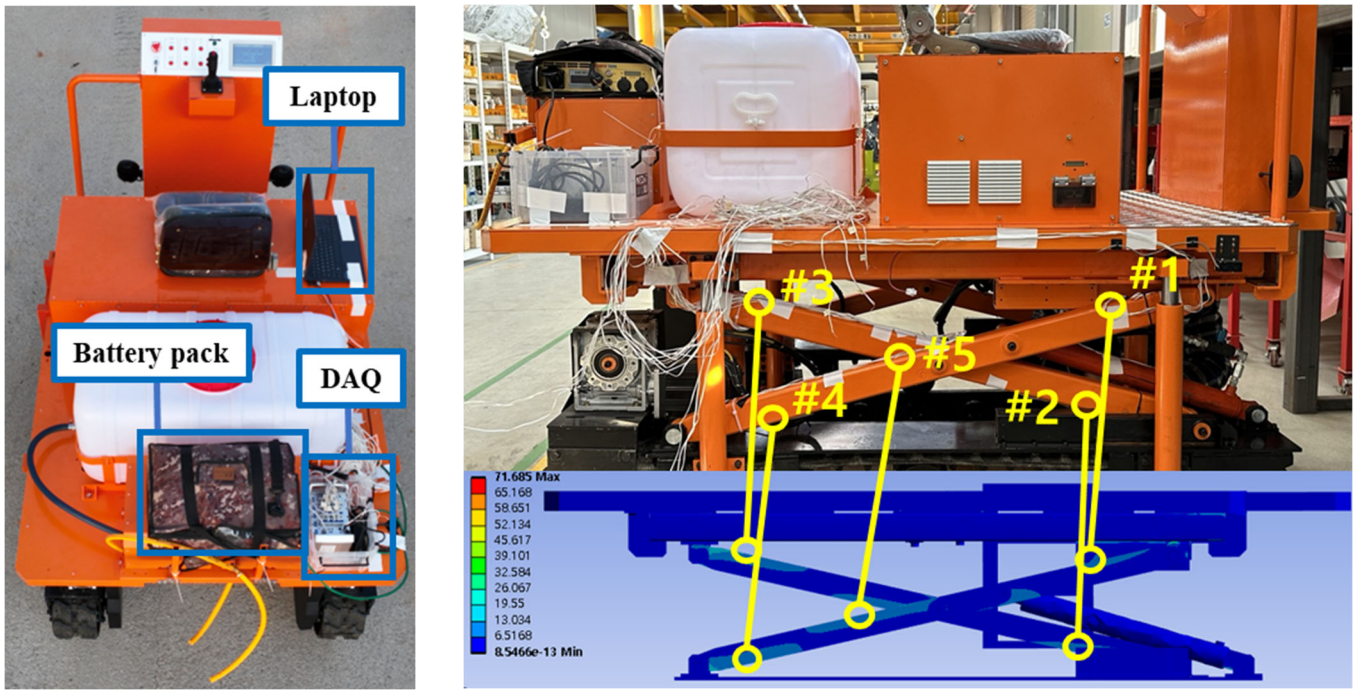

(**a**) (**b**)

Figure 4. Measurement system: (**a**) laptop, battery pack, and DAQ; (**b**) strain gauge attachment point (#1, #2, #3, #4, #5 are weak points).

Figure 5 shows the strain gauges used in this study in the form of a triaxial rosette positioned at 0°/90°/45° angles. The strain gauge has a gage factor of 2.11 ± 1.0%, a gage length of 1 mm, and a gage resistance of 350.0 Ω ± 0.7%. Triaxial strain gauges are attached where the main load direction is not obvious [33].

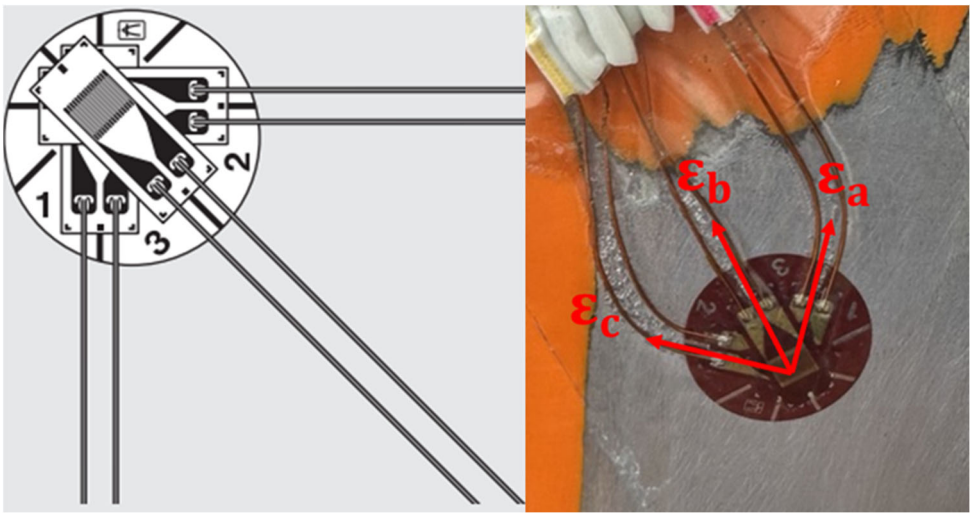

Figure 5. Triaxial, 0°/90°/45° stacked rosette strain gauge (ε is strain value).

2.2.3. Measurement Conditions

The test was conducted on a field and a paved road in Hada, Iksan, Jeollabuk-do, Korea. The location of the field and pavement is 35°59′24.77 N, 127°1′18.79 E, as shown in Figure 6. The cultivation tractor used in this study was designed to have an adjustable width to accommodate various agricultural tasks. Therefore, the width was set to two conditions:

maximum and minimum. As shown in Figure 2, the maximum width is 1040 mm, and the minimum width is 790 mm. Considering the working environment of the cultivation tractor, the soil conditions were set to paved road and field. Driving was measured in forward and reverse. The test distance was established at 20 m, and the driving speed was set at 0.2 m/s, considering the development stage of the cultivation tractor. The test was repeated three times for each condition, and the average of the three times was used.

Figure 6. Test field: (**a**) paved road; (**b**) farm field.

2.3. Safety Analysis Methods

The analysis process is shown in Figure 7. After measuring stress data in the time domain, the data with irregular amplitudes were used to calculate cycles using rainflow counting. Based on these calculated cycles, cumulative damage was analyzed using the Palmgren–Miner rule [31,32] to predict fatigue life. The spreadsheet software Excel (Microsoft 365) was utilized for the conversion calculations. Rainflow counting, cumulative damage analysis, and fatigue life prediction were analyzed using the commercial program nCode (HBM, Darmstadt, Germany).

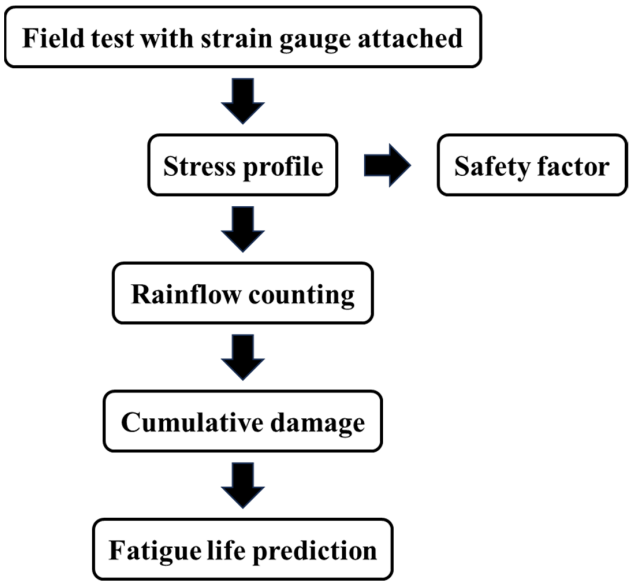

Figure 7. Flow chart for fatigue life prediction.

2.3.1. Stress Profile

A triaxial strain gauge can be used to measure strain (ε_a, ε_b, ε_c) in three directions, as shown in Figure 5. Using the strain data, the maximum principal stress, minimum principal stress, and von Mises stress can be calculated using Equations (1)–(3).

$$\sigma_{max} = \frac{E}{2(1-\nu^2)}[(1+\nu)(\varepsilon_a+\varepsilon_c) + (1-\nu)\sqrt{2(\varepsilon_a-\varepsilon_b)^2+(\varepsilon_b-\varepsilon_c)^2}] \quad (1)$$

$$\sigma_{min} = \frac{E}{2(1-\nu^2)}[(1+\nu)(\varepsilon_a+\varepsilon_c) - (1-\nu)\sqrt{2(\varepsilon_a-\varepsilon_b)^2+(\varepsilon_b-\varepsilon_c)^2}] \quad (2)$$

$$\sigma_{vm} = \sqrt{\sigma_{max}^2 - \sigma_{max}\sigma_{min} + \sigma_{min}^2} \quad (3)$$

where σ_{max} is the maximum principal stress, σ_{min} is the minimum principal stress, ν is Poisson's ratio, E is Young's modulus, and σ_{vm} is von Mises stress.

2.3.2. Safety Factor

In mechanical design, it is essential to consider uncertainties, such as material strength, machining precision, and workload, to ensure high safety beyond the performance or capability required by the designed product. The safety of a machine under load is evaluated using a safety factor. A higher safety factor leads to increased cost and weight, while a lower safety factor increases the risk to safety. Therefore, the safety factor must be determined by considering not only structural safety but also economic and usability aspects. The safety factor is defined, as shown in Equation (4), as the ratio of the yield stress that the structure can withstand to the expected maximum stress acting on the structure.

$$SF = \frac{\sigma_{yield}}{\sigma_{vm}} \quad (4)$$

where SF is the safety factor and σ_{yield} is the yield stress.

If the safety factor calculated for the maximum stresses encountered during operation is greater than or equal to 1.0, the design is considered safe. On the other hand, if the safety factor is less than 1.0, the design is considered unsafe, meaning that it could cause breakage or failure of the part [34]. In general, the safety factor applied by the machine is between 1.2 and 1.4.

2.3.3. Rainflow Counting

When the cultivation tractor is operating, it is subjected to irregular amplitude loads rather than constant amplitude loads. In order to convert these irregular amplitude loads into regular amplitude cycles, cycle counting is required. There are many methods for cycle counting, such as level-crossing counting, peak counting, simple-range counting, and rainflow counting [35,36]. Among them, the rainflow counting method is commonly used [37,38]. This method identifies load cycles within complex loading histories, analyzing the range (amplitude) and mean of the load for each cycle to calculate fatigue damage. Here, a cycle refers to the process starting from the application of the load to a body to its full release. Rainflow counting is especially useful for predicting the fatigue life of structures or mechanical components subjected to variable loading.

2.3.4. Analysis of Cumulative Damage

Most fatigue data are based on constant amplitude testing. However, in the working environment of a real machine, irregular load amplitudes occur. This makes the direct use of S–N curves difficult. Instead, a method has been devised that utilizes the S–N curve and can be applied under irregular load amplitude conditions. This method is cumulative damage. One such cumulative damage theory is the Palmgren–Miner rule, a linear damage rule developed by Palmgren and Miner. This rule is useful for predicting the fatigue life of components exposed to irregular load amplitudes using constant amplitude data, and it is

used in conjunction with cycle counting methods to provide an estimate of life. Equation (5) is the Palmgren–Miner rule. When $D_t \geq 1$, failure occurs.

$$D_t = \sum_{i=1}^{k} \frac{n_i}{N_i} \tag{5}$$

where D_t is the total damage, n_i is the number of applied cycles, and N_i is the number of cycles to failure.

2.3.5. Fatigue Life Prediction

The S–N curve of stainless steel 400, i.e., the weak point material, can be represented by calculating the fatigue strength for 10^3 cycles and 10^6 cycles using Equations (6) and (7) [39].

$$S_f = 0.75UTS \tag{6}$$

where S_f is the 10^3 cycle strength and UTS is the ultimate tensile strength.

$$S_n = 0.5UTS \times C_L C_G C_S C_T C_R \tag{7}$$

where S_n is the 10^6 cycle strength, C_L is the load factor, C_G is the gradient factor, C_S is the surface factor, C_T is the temperature factor, and C_R is the reliability factor.

The fatigue life is calculated via Equation (8).

$$L_f = \frac{1}{D_t} \times t \tag{8}$$

where L_f is the fatigue life and t is the time.

3. Results and Discussion

3.1. Stress Measurement

The von Mises stresses at the strain gauge attachment points for each condition of paved road/farm field, maximum/minimum width, and forward/backward are shown in Figure 8. The maximum von Mises stress and average von Mises stress at each point are shown in Table 3. The average von Mises stress during driving was the greatest at point #1, but the maximum von Mises stress during driving, 83.22 MPa, occurred at point #5.

The average von Mises stress values measured at points #1, #2, #3, #4, and #5 were 33.64 MPa, 12.46 MPa, 25.50 MPa, 11.51 MPa, and 32.60 MPa, respectively, demonstrating observed stress differences based on location. However, the stress difference when conditions at the same location changed was minimal, as indicated in Table 3. The small stress difference is attributed to the slow driving speed of the cultivation tractor, which is assessed as not causing significant variations.

The average values of the standard deviation of the stresses measured at points #1, #2, #3, #4, and #5 were 2.21, 2.14, 0.81, 0.73, and 9.75, respectively. This indicates that the rear part of the manager was relatively more stable compared to the front part. In particular, point #5, where the two links connect, emerged as the most unstable location. Distinct from other points, point #5 is significantly distanced from the connection point of the driving section or plate, which is judged to be relatively unstable.

The average stresses measured at points #1 and #3 were higher than the average stresses at points #2 and #4, indicating that the upper part of the vulnerable area was subjected to higher loads than the lower part.

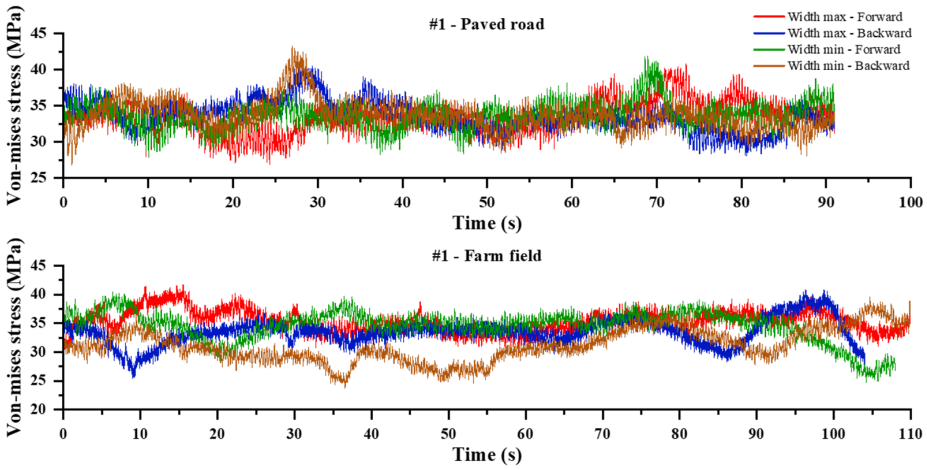

(**a**)

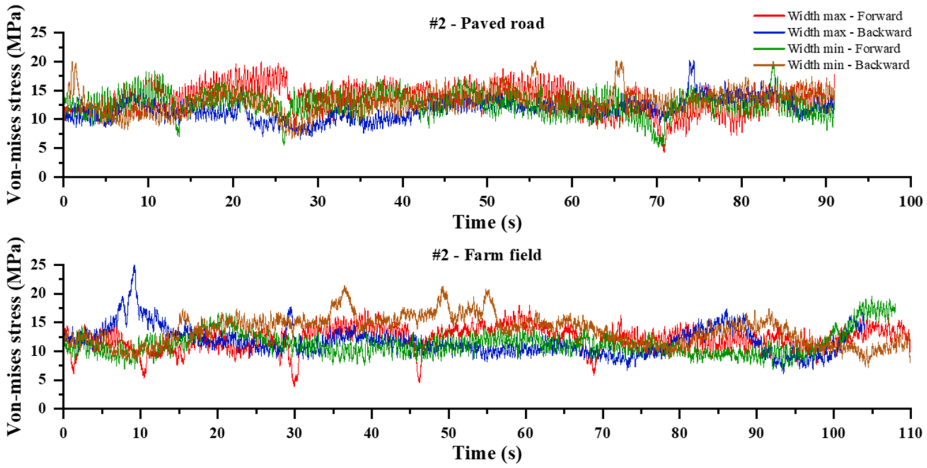

(**b**)

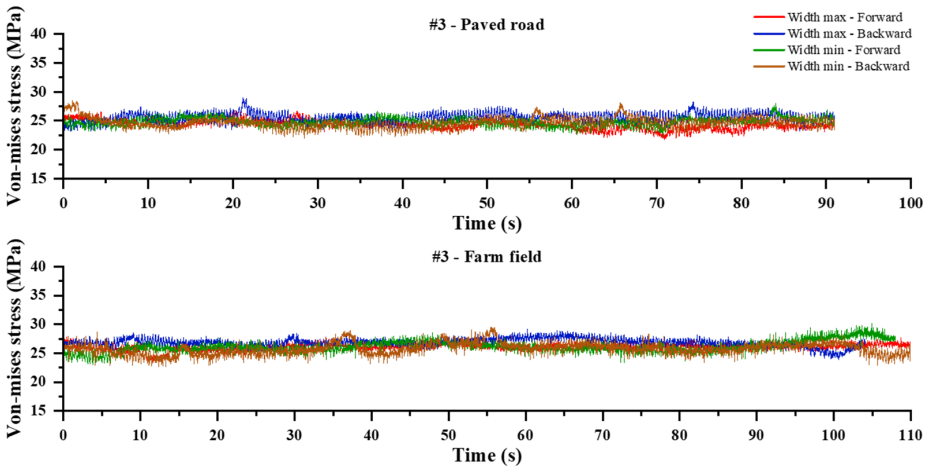

(**c**)

Figure 8. *Cont.*

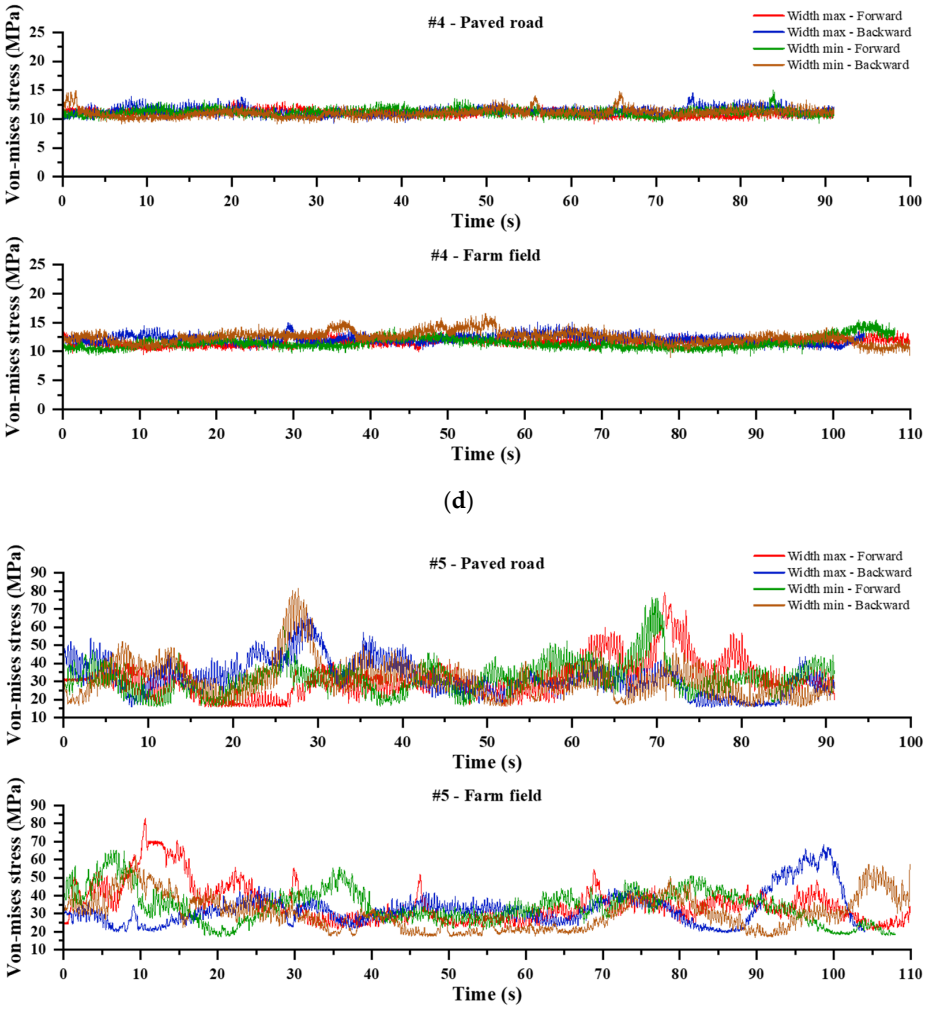

Figure 8. von Mises stress attachment point: (**a**) #1; (**b**) #2; (**c**) #3; (**d**) #4; (**e**) #5.

Table 3. Stress measurement results by conditions.

Soil Condition	Width	Drive	Attachment Point	Maximum Stress (MPa)	Average Stress (MPa)	Standard Deviation
Paved road	Max	Forward	#1	40.83	33.43	2.09
			#2	20.04	13.45	2.35
			#3	26.74	24.35	0.78
			#4	13.34	11.00	0.53
			#5	79.05	31.56	10.26
		Backward	#1	40.53	33.62	2.05
			#2	20.25	11.78	1.77
			#3	28.98	25.43	0.86
			#4	14.57	11.29	0.67
			#5	67.78	32.48	9.59
	Min	Forward	#1	41.88	33.74	1.79
			#2	20.07	12.66	1.99
			#3	28.07	24.81	0.68
			#4	15.06	11.15	0.61
			#5	76.40	31.93	8.90
		Backward	#1	43.22	33.70	2.03
			#2	20.20	13.04	2.01
			#3	28.47	24.64	0.91
			#4	14.95	11.05	0.73
			#5	81.29	31.21	10.21

Table 3. *Cont.*

Soil Condition	Width	Drive	Attachment Point	Maximum Stress (MPa)	Average Stress (MPa)	Standard Deviation
Farm field	Max	Forward	#1	41.67	35.36	1.88
			#2	18.03	12.14	2.04
			#3	27.86	26.12	0.54
			#4	13.83	11.59	0.58
			#5	83.22	35.56	10.70
		Backward	#1	40.88	33.48	2.23
			#2	25.37	11.70	2.39
			#3	29.18	26.82	0.70
			#4	15.13	12.14	0.71
			#5	68.29	32.71	9.25
	Min	Forward	#1	40.45	34.52	2.66
			#2	19.59	11.32	2.05
			#3	30.17	26.12	0.97
			#4	15.47	11.47	0.95
			#5	65.22	34.38	9.38
		Backward	#1	39.56	31.29	2.97
			#2	21.52	13.55	2.54
			#3	29.60	25.74	1.00
			#4	16.63	12.40	1.07
			#5	61.52	30.88	9.72

3.2. Safety Analysis

3.2.1. Safety Factor

The material of the stress measurement point was stainless steel 400 with a yield strength of 250 MPa, and the safety factor was derived using Equation (4). The derived safety factors for each condition are shown in Table 4. The safety factors derived for all test conditions ranged from 3.00 to 18.74. The safety factor for point #1 was 5.78–6.32; for point #2, it was 9.85–13.87; for point #3, it was 8.29–9.35; for point #4, it was 15.03–18.74; and for point #5, it was 3.08–4.06. The maximum stresses at points #2 and #4 were lower, resulting in higher safety factors than other locations. For all test conditions, the safety factor was above 1.0, and the design was considered safe. This exceeded the 1.2–1.4 that is typically applied when designing a machine. Having an excessively high safety factor can lead to issues, such as increased costs, added weight, decreased energy efficiency, resource wastage, and reduced design flexibility. The use of more materials or more expensive materials escalates costs and can negatively impact the performance of a machine due to increased weight, requiring more energy for transportation and movement. This signifies a waste of resources and may not align with sustainability goals. Therefore, it is crucial to ensure the safety of the machine while also considering the balance between cost, weight, energy efficiency, and resource usage.

3.2.2. Rainflow Counting

In #1, the mean stress value was 25–40 MPa, and the stress amplitude was 0–20 MPa. The mean stress value at #2 was 0–25 MPa, and the stress amplitude was 0–20 MPa. The mean stress value at #3 was 22–30 MPa, and the stress amplitude was 0–8 MPa. The mean stress value at #4 was 9–16 MPa, and the stress amplitude was 0–8 MPa. The mean stress value at #5 was 10–80 MPa, and the stress amplitude was 0–65 MPa. Point #5 had the largest standard deviation and therefore the widest range of mean stress and stress amplitude.

Table 4. Safety factor results by conditions.

Soil Condition	Width	Drive	Attachment Point	Safety Factor
Paved road	Max	Forward	#1	6.12
			#2	12.48
			#3	9.35
			#4	18.74
			#5	3.16
		Backward	#1	6.17
			#2	12.35
			#3	8.63
			#4	17.16
			#5	3.69
	Min	Forward	#1	5.97
			#2	12.49
			#3	8.91
			#4	16.60
			#5	3.27
		Backward	#1	5.78
			#2	12.38
			#3	8.78
			#4	16.72
			#5	3.08
Farm field	Max	Forward	#1	6.00
			#2	13.87
			#3	8.97
			#4	18.08
			#5	3.00
		Backward	#1	6.12
			#2	9.85
			#3	8.57
			#4	16.52
			#5	3.66
	Min	Forward	#1	6.18
			#2	12.76
			#3	8.29
			#4	16.16
			#5	3.83
		Backward	#1	6.32
			#2	11.62
			#3	8.45
			#4	15.03
			#5	4.06

3.2.3. Cumulative Damage

Table 5 shows the cumulative damage derived for each condition by attachment location. When the cumulative damage value reaches 1, breakage occurs. The maximum cumulative damage for each location (#1, #2, #3, #4, and #5) was 2.6257×10^{-12}, 4.0895×10^{-12}, 5.1469×10^{-14}, 3.2016×10^{-14}, and 6.8551×10^{-9}. The largest cumulative damage occurred at #5. Figure 9 shows the rainflow counting result and cumulative damage result for the #5 points. The cycle that caused the maximum damage occurred only once, yet it constituted over 80% of the total damage. Thus, it was evident that certain loads significantly influence damage and fatigue life.

Table 5. Total damage by conditions.

Soil Condition	Width	Drive	Attachment Point	Total Damage
Paved road	Max	Forward	#1	1.2870×10^{-12}
			#2	1.9935×10^{-12}
			#3	4.6008×10^{-15}
			#4	2.4073×10^{-15}
			#5	5.4845×10^{-9}
		Backward	#1	6.5743×10^{-13}
			#2	6.3014×10^{-13}
			#3	1.9754×10^{-14}
			#4	9.0261×10^{-15}
			#5	2.1077×10^{-9}
	Min	Forward	#1	1.5756×10^{-12}
			#2	1.7317×10^{-12}
			#3	8.2830×10^{-15}
			#4	9.0922×10^{-15}
			#5	4.7998×10^{-9}
		Backward	#1	2.6257×10^{-12}
			#2	1.1076×10^{-12}
			#3	2.4692×10^{-14}
			#4	1.4300×10^{-14}
			#5	6.8551×10^{-9}
Farm field	Max	Forward	#1	6.5306×10^{-13}
			#2	1.4521×10^{-15}
			#3	1.9400×10^{-15}
			#4	3.7340×10^{-15}
			#5	5.1304×10^{-9}
		Backward	#1	1.6010×10^{-12}
			#2	4.0895×10^{-12}
			#3	5.1999×10^{-15}
			#4	9.2171×10^{-15}
			#5	1.1143×10^{-9}
	Min	Forward	#1	1.9594×10^{-12}
			#2	5.3740×10^{-13}
			#3	2.7410×10^{-14}
			#4	1.2392×10^{-14}
			#5	1.3162×10^{-9}
		Backward	#1	1.7861×10^{-12}
			#2	8.5055×10^{-13}
			#3	5.1469×10^{-14}
			#4	3.2016×10^{-14}
			#5	9.2685×10^{-10}

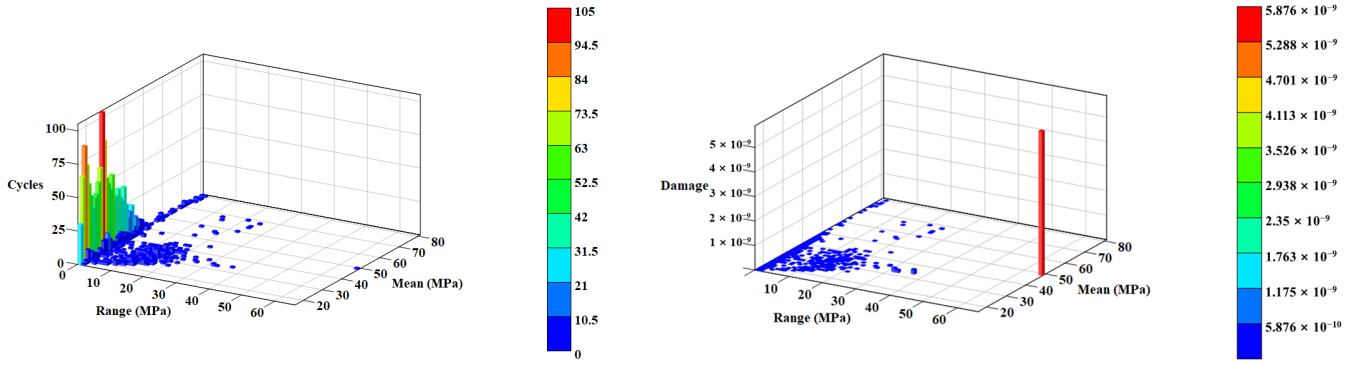

(**a**) (**b**)

Figure 9. Histogram of maximum cumulative damage point (#5/paved road/width minimum/backward): (**a**) rainflow counting result; (**b**) cumulative damage result.

3.2.4. Fatigue Life Prediction

The fatigue strengths of stainless steel 400 for 10 and 11 cycles are =315 MPa and =92.3013 MPa from Equations (6) and (7). Based on these results, the S–N curve for stainless steel 400 is shown in Figure 10.

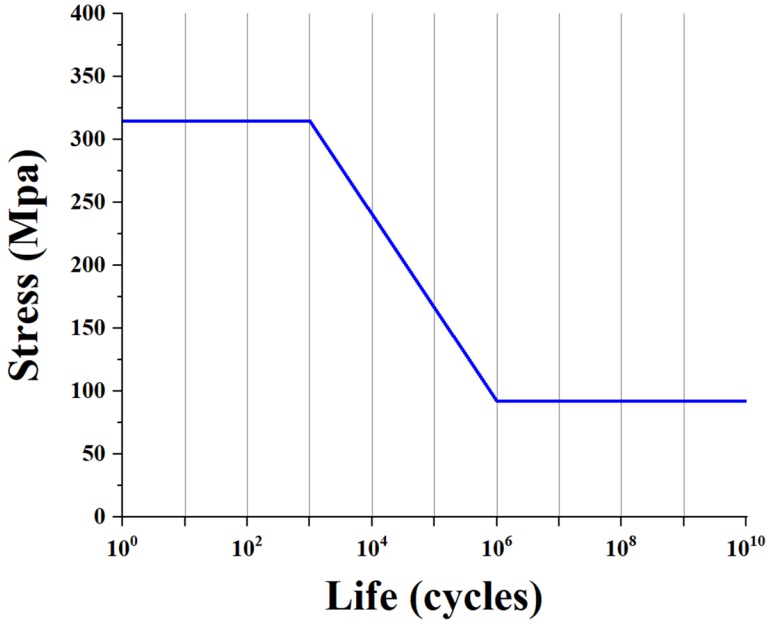

Figure 10. S–N curve for stainless steel 400.

In Korea, the cultivation tractor was found to have 29.7 h of use per year. When comparing fatigue life predictions considering annual hours of use, the lowest predicted value was 124,176 years. Although the prediction is considered too large, it seems to be a reasonable prediction based on the results of previous studies [40,41]. With a service life of 5 years, the cultivation tractor can be safely used for the duration of the service life.

4. Conclusions

In this study, the stresses generated in the frame of an electrically driven, multipurpose cultivation tractor were measured during operation to evaluate the safety factor and fatigue life. A measurement system based on strain gauges was built, and experiments were conducted by varying the width (maximum/minimum), soil (pavement/farm field), and driving (forward/backward) conditions of the cultivation tractor.

1. When measuring the stresses at the strain gauge attachment locations, the average von Mises stress was greatest at #1. However, the maximum von Mises stress of 83.2 MPa was measured at #5. At all other locations (#1, #2, #3, and #4) except #5, the standard deviation of the stresses was 2.97 MPa or less, indicating that the stresses were measured almost uniformly.
2. The safety factors calculated through the formulas range from 3.00 to 18.74 for all test conditions, which suggests that the machine design is deemed safe as it is above 1.0. However, these values exceed the typical safety factor range of 1.2 to 1.4 usually applied in machine design. Consequently, an excessively high safety factor calls for a reevaluation from an economic perspective.
3. Rainflow counting was analyzed to show the range of stress levels in each condition. The range of mean stress and amplitude at #5 was wider than at other locations.
4. Analysis of the rainflow counting histogram and cumulative damage histogram shows that most stress cycles occur at small stress ranges and small mean stresses. Large stress ranges and large mean stresses do not show many cycles. Although the number of cycles is small, stresses with large stress ranges and large mean stresses cause the most damage.
5. The cultivation tractor is used for 29.7 h per year, which gives a fatigue life estimate of at least 124,176 years. Therefore, it is expected to be safely used for the service life of the machine.

In this study, we performed load measurement experiments at a driving speed of 0.2 m/s, considering the manufacturing phase of a cultivation tractor. In future studies, we plan to evaluate performance under worst-case conditions by increasing the driving speed and conducting experiments under the maximum load required for the tractor to perform its tasks.

Author Contributions: Conceptualization, J.-S.N. and C.-S.S.; methodology, J.-S.N. and C.-S.S.; software, I.-S.H. and J.-H.K.; validation, I.-S.H. and W.-T.I.; formal analysis, I.-S.H.; investigation, I.-S.H. and W.-T.I.; resources, H.-H.J.; data curation, I.-S.H.; writing—original draft preparation, I.-S.H.; writing—review and editing, I.-S.H., W.-T.I. and C.-S.S.; visualization, I.-S.H.; supervision, C.-S.S.; project administration, C.-S.S.; funding acquisition, C.-S.S. All authors have read and agreed to the published version of the manuscript.

Funding: This work was supported by the Korea Institute of Planning and Evaluation for Technology in Food, Agriculture, Forestry (IPET) through the Eco-friendly Power Source Application Agricultural Machinery Technology Development Program, funded by the Ministry of Agriculture, Food and Rural Affairs (MAFRA) (RS-2022-IP322044). The results are from a study from the "Leaders in INdustry-university Cooperation 3.0" Project, supported by the Ministry of Education and the National Research Foundation of Korea.

Data Availability Statement: No new data were created or analyzed in this study.

Conflicts of Interest: Author Hwan-Hong Jeung was employed by the company Cheung Won SFA Co., Ltd. The remaining authors declare that the research was conducted in the absence of any commercial or financial relationships that could be construed as a potential conflict of interest.

References

1. Woodsong, C. Old farmers, invisible farmers: Age and agriculture in Jamaica. *J. Cross-Cult. Gerontol.* **1994**, *9*, 277–299. [CrossRef]
2. Pantić, M.; Živanović-Miljković, J. Regional differences between rural areas of Serbia in population aging and agricultural activities: Case studies of the Inđija and Knjaževac municipalities. *Spatium* **2010**, *22*, 29–37. [CrossRef]
3. Guo, G.; Wen, Q.; Zhu, J. The Impact of Aging Agricultural Labor Population on Farmland Output: From the Perspective of Farmer Preferences. *Math. Probl. Eng.* **2015**, *2015*, 730618. [CrossRef]
4. Wirotsattabut, C.; Suphannachart, W.; Praneetvatakul, S. Effect of aging society on labor productivity in Thai agriculture. *Kaen Kaset Khon Kaen Agric. J.* **2021**, *47*, 419–432. [CrossRef]
5. Shen, D.; Liang, H.; Shi, W. Rural Population Aging, Capital Deepening, and Agricultural Labor Productivity. *Sustainability* **2023**, *15*, 8331. [CrossRef]
6. Li, H.; Zhou, X.; Tang, M.; Guo, L. Impact of Population Aging and Renewable Energy Consumption on Agricultural Green Total Factor Productivity in Rural China: Evidence from Panel VAR Approach. *Agriculture* **2022**, *12*, 715. [CrossRef]

7. Liao, L.; Long, H.; Gao, X.; Ma, E. Effects of land use transitions and rural aging on agricultural production in China's farming area: A perspective from changing labor employing quantity in the planting industry. *Land Use Policy* **2019**, *88*, 104152. [CrossRef]
8. Lee, R.; Mason, A. Fertility, Human Capital, and Economic Growth over the Demographic Transition. *Eur. J. Popul. Rev. Eur. Démographie* **2010**, *26*, 159–182. [CrossRef]
9. Kim, Y.C.; Kim, D.S.; Park, K.H.; Kim, D.S. A Study on Analysis of Industrial Injury Characteristics of Aging Workers in Agriculture. *J. Ergon. Soc. Korea* **2014**, *33*, 477–486. [CrossRef]
10. Merisalu, E.; Leppälä, J.; Jakob, M.; Rautiainen, R. Variation in Eurostat and national statistics of accidents in agriculture. *Agron. Res.* **2019**, *17*, 1969–1983. [CrossRef]
11. Swe, K.M.; Islam, M.N.; Chowdhury, M.; Ali, M.; Wing, S.; Jun, H.J.; Lee, S.H.; Chung, S.O.; Kim, D.G. Theoretical analysis of power requirement of a four-row tractor-mounted Chinese cabbage collector. *J. Biosyst. Eng.* **2021**, *46*, 139–150. [CrossRef]
12. Lu, X.; Zheng, S. Changes in mechanical properties of vehicle components after strengthening under low-amplitude loads below the fatigue limit. *Fatigue Fract. Eng. Mater. Struct.* **2009**, *32*, 847–855. [CrossRef]
13. Wöllner, U.; Szlosarek, R.; Kröger, M. Fatigue behavior of agricultural rims under rotating bending load. *Fatigue Fract. Eng. Mater. Struct.* **2022**, *45*, 2143–2158. [CrossRef]
14. Barna, R.A.; Popovych, P.V. Influence of Operating Media on the Fatigue Fracture of Steels for Elements of Agricultural Machines. *Mater. Sci.* **2014**, *50*, 377–380. [CrossRef]
15. Kim, J.-H.; Sri, M.; Hwang, S.-J.; Jang, M.-K.; Kim, S.-J.; Yang, Y.-J.; Nam, J.-S. Safety Analysis of Fastening Device of Agricultural By-Product Collector in Various Ground Conditions. *Agriculture* **2023**, *13*, 2064. [CrossRef]
16. Baek, S.H.; Cho, S.S.; Joo, W.S. Fatigue life prediction based on the rainflow cycle counting method for the end beam of a freight car bogie. *Int. J. Automot. Technol.* **2008**, *9*, 95–101. [CrossRef]
17. Djebli, A.; Aid, A.; Bendouba, M.; Amrouche, A.; Benguediab, M.; Benseddiq, N. A non-linear energy model of fatigue damage accumulation and its verification for Al-2024 aluminum alloy. *Int. J. Non-Linear Mech.* **2013**, *51*, 145–151. [CrossRef]
18. Cui, W.; Wang, F.; Huang, X. A unified fatigue life prediction method for marine structures. *Mar. Struct.* **2011**, *24*, 153–181. [CrossRef]
19. Kebir, T.; Correia, J.; Benguediab, M.; de Jesus, A.M.P. Numerical study of fatigue damage under random loading using rainflow cycle counting. *Int. J. Struct. Integr.* **2021**, *12*, 149–162. [CrossRef]
20. Faria, R.; Moura, P.; Delgado, J.; de Almeida, A.T. A sustainability assessment of electric vehicles as a personal mobility system. *Energy Convers. Manag.* **2012**, *61*, 19–30. [CrossRef]
21. Willems, F.; Foster, D. Integrated Powertrain Control to meet future CO_2 and Euro-6 emissions targets for a diesel hybrid with SCR-deNOx system. In Proceedings of the 2009 American Control Conference, St. Louis, MO, USA, 10–12 June 2009; pp. 3944–3949. [CrossRef]
22. Desantes, J.M.; Molina, S.; Novella, R.; Lopez-Juarez, M. Comparative global warming impact and NOX emissions of conventional and hydrogen automotive propulsion systems. *Energy Convers. Manag.* **2020**, *221*, 113137. [CrossRef]
23. Borghi, M.; Zardin, B.; Pintore, F.; Belluzzi, F. Energy Savings in the Hydraulic Circuit of Agricultural Tractors. *Energy Procedia* **2014**, *45*, 352–361. [CrossRef]
24. Martinho, V.J.P.D. Energy consumption across European Union farms: Efficiency in terms of farming output and utilized agricultural area. *Energy* **2016**, *103*, 543–556. [CrossRef]
25. Shin, C.S.; Kim, K.U.; Kwon, P. Economic Analysis of Agricultural Tractors in South Korea: Classified Based on Energy Efficiency Grades. *Appl. Eng. Agric.* **2017**, *33*, 667–677. [CrossRef]
26. Shin, C.S.; Kim, K.U. CO_2 Emissions by Agricultural Machines in South Korea. *Appl. Eng. Agric.* **2018**, *34*, 311–315. [CrossRef]
27. Troncon, D.; Alberti, L. Case of Study of the Electrification of a Tractor: Electric Motor Performance Requirements and Design. *Energies* **2020**, *13*, 2197. [CrossRef]
28. Das, A.; Jain, Y.; Agrewale, M.R.B.; Bhateshvar, Y.K.; Vora, K. Design of a Concept Electric Mini Tractor. In Proceedings of the 2019 IEEE Transportation Electrification Conference (ITEC-India), Bengaluru, India, 17–19 December 2019; pp. 1–5. [CrossRef]
29. He, L.; Gu, L.; Kong, L.; Gu, Y.; Liu, C.; He, T. Exploring Adaptive Reconfiguration to Optimize Energy Efficiency in Large-Scale Battery Systems. In Proceedings of the 2013 IEEE 34th Real-Time Systems Symposium, Vancouver, BC, Canada, 3–6 December 2013; pp. 118–127. [CrossRef]
30. Burd, J.T.J.; Moore, E.A.; Ezzat, H.; Kirchain, R.; Roth, R. Improvements in electric vehicle battery technology influence vehicle lightweighting and material substitution decisions. *Appl. Energy* **2021**, *283*, 116269. [CrossRef]
31. Palgren, A. Die lebensdauer von kugellagern. *Verfahrenstechnik Berl.* **1924**, *68*, 339–341.
32. Miner, M.A. Cumulative Damage in Fatigue. *J. Appl. Mech.* **1945**, *12*, A159–A164. [CrossRef]
33. Sri, M.; Hwang, S.J.; Nam, J.S. Experimental safety analysis of transplanting device of the cam-type semi-automatic vegetable transplanter. *J. Terramechanics* **2022**, *103*, 19–32. [CrossRef]
34. Knabner, D.; Hauschild, S.; Suchý, L.; Vetter, S.; Leidich, E.; Hasse, A. Calculation method for the fail-safe design of steel-steel contacts subject to fretting fatigue based on a worst-case assumption. *Int. J. Fatigue* **2022**, *165*, 107217. [CrossRef]
35. Downing, S.D.; Socie, D.F. Simple rainflow counting algorithms. *Int. J. Fatigue* **1982**, *4*, 31–40. [CrossRef]
36. Rychlik, I. A new definition of the rainflow cycle counting method. *Int. J. Fatigue* **1987**, *9*, 119–121. [CrossRef]
37. He, L.; Xu, L.; Itoh, T. Novel fatigue life prediction approach combined with rain-flow cycle counting process for random multiaxial non-proportional loading. *Fatigue Fract. Eng. Mater. Struct.* **2023**, *46*, 4392–4405. [CrossRef]

38. Li, Y.; Jin, A.; Dai, Y.; Yang, D.; Zheng, B. Prediction of Remaining Fatigue Life of In-Service Bridge Cranes. *Appl. Sci.* **2023**, *13*, 12250. [CrossRef]
39. Juvinall, R.C.; Marshek, K.M. *Fundamentals of Machine Component Design*; John Wiley & Sons: Hoboken, NJ, USA, 2020.
40. Markumningsih, S.; Hwang, S.-J.; Kim, J.-H.; Jang, M.-K.; Nam, J.-S. Stress Simulation on Four-Bar Link-Type Transplanting Device of Semiautomatic Vegetable Transplanter. *Agriculture* **2024**, *14*, 42. [CrossRef]
41. Paraforos, D.S.; Griepentrog, H.W.; Vougioukas, S.G.; Kortenbruck, D. Fatigue life assessment of a four-rotor swather based on rainflow cycle counting. *Biosyst. Eng.* **2014**, *127*, 1–10. [CrossRef]

Disclaimer/Publisher's Note: The statements, opinions and data contained in all publications are solely those of the individual author(s) and contributor(s) and not of MDPI and/or the editor(s). MDPI and/or the editor(s) disclaim responsibility for any injury to people or property resulting from any ideas, methods, instructions or products referred to in the content.